



NEUTRON SCATTERING IN STUDIES OF COMPLEX ANISOTROPIC MICROSTRUCTURES

J. MATĚJÍČEK¹, J. ILAVSKÝ² AND T. GNÄUPEL-HEROLD³

¹*Institute of Plasma Physics, Za Slovankou 3, 18221 Praha, Czech Republic*

²*University of Maryland at College Park, College Park, MD 20742, USA*

³*National Institute of Standards and Technology, 100 Bureau Dr., Gaithersburg, MD 20899,
USA*

ABSTRACT

Wide industrial application of complex anisotropic microstructures, such as those of thermally sprayed deposits, requires development and utilization of novel characterization techniques. These techniques must be able to reflect the anisotropy of the microstructure. Further, it is often necessary to be able to study materials in situ, without sample removal and preparation. Also due to fragility of the materials many standard techniques fail. We present an overview of neutron scattering techniques – anisotropic small-angle neutron scattering used for characterization of void microstructures and neutron diffraction used for characterization of elastic constants and residual stress. Both techniques avoid some of the disadvantages of standard techniques – cross sectional microscopy and X-ray diffraction, respectively; however, their results may be presented in somehow less than usual manner. Results obtained on metallic (Ni-based) and ceramic (yttria-stabilized zirconia) deposits are compared with results obtained with standard techniques. Our conclusions show that the results of standard techniques – treated with caution – should be complemented with the techniques presented to obtain fuller microstructure and properties characterization. Such characterization can be then more reliably used in deposits development.

KEYWORDS

Neutron scattering, neutron diffraction, thermally sprayed coatings, anisotropy, void structure, elastic properties, residual stress.

INTRODUCTION

Thermally sprayed deposits find numerous applications as thermal barrier, wear- and corrosion-protective coatings as well as free-standing components of various shapes and sizes. The material to be deposited – in the form of powder or wire – is melted by means of plasma jet, combustion flame or electric arc [1]. Then the jet transports the molten particles towards the substrate where they impact, spread and solidify. The deposit thus formed consists of a multitude of individual lamellar particles – “splats” (see Fig. 1). This unique structure gives the deposit specific properties, including anisotropy, porosity and thermal and mechanical properties markedly different from a bulk material of the same composition. High temperature excursions lead to significant residual stresses. All of these factors play important role in the deposit applicability and lifetime in service.

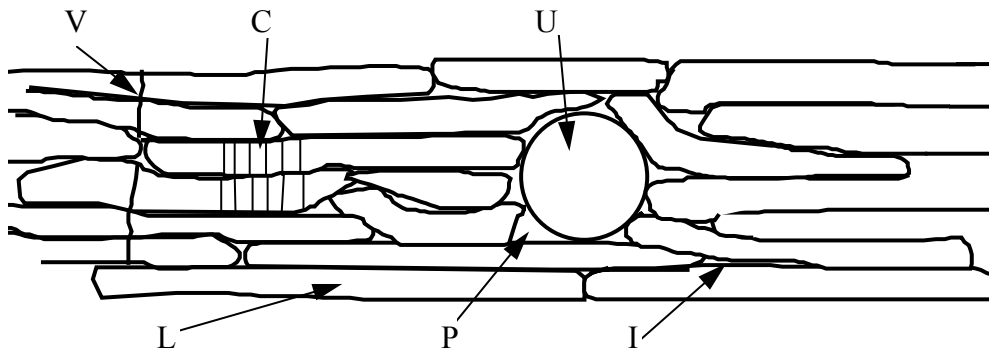


Fig. 1. Schematic of thermal spray coating with characteristic microstructural features: L = lamella (splat) formed from a single droplet, U = unmelted particle, embedded in the coating, P = volumetric pore, I = area of imperfect contact between lamellae (horizontal crack, interlamellar pore), V = large vertical crack, C = columnar grain structure (only shown in small region). For example of a real structure, see Fig. 2.

The *void system* in a thermally sprayed deposit can be divided into several subsystems. The volumetric pores originate from incomplete filling of the surface roughness by the molten material (e.g., around spherical unmelted particles or inclusions) or from gas evaporation from the molten phase. They usually account for the largest portion of porosity volume, but their contribution to the total pore surface area is small. Interlamellar voids are generated when adjacent lamellae do not form an intimate contact (e.g., due to insufficient wetting) with each other or when the coating cracks under compressive or shear stresses acting parallel with the substrate. These thin, flat voids have a dominant orientation parallel to the substrate. Their largest dimension is comparable to the splat width (order of 100 μm). Intralamellar cracks are generated by tensile stress acting parallel with the substrate, due to rapid cooling of the deposited material after impact. Their largest dimension is comparable to the splat thickness (order of μm) and their dominant orientation is perpendicular to the substrate. Although the last two void systems represent only a small part of the total porosity volume, they are major contributors of the total surface area. Due to their shape anisotropy and preferred orientation, these have the strongest influence on thermal and mechanical properties of the deposits [2].

The *elastic constants* are affected by the deposit structure on both macro- and microscopic levels. Simply the presence of porosity would reduce the elastic constants of thermally sprayed deposits compared to their bulk counterparts. However, the porosity is typically below 10 %, while the elastic constants generally range from 5 to 50 % of the corresponding bulk values [1,3]. This is a consequence of the anisotropic shape of the voids. Experimental observations show that Young's modulus perpendicular to the coating plane is generally lower than in the coating plane. This has been explained by the large interlamellar voids which open under tensile stress and enable the lamellae to bend, thus providing an additional strain component [4]. Upon unloading, this process reverses, giving rise to non-linear elastic behavior. In the in-plane direction, the major factor are the (vertical) cracks. These have smaller lateral dimension, thus such an effect would be less pronounced. Additionally, the lamellae are interlocked like a jigsaw puzzle and the modulus is affected by frictional forces and shear deformation in the regions of true contact. Under compressive stress, the voids and cracks start to close, bringing the solid material into contact. This leads to an increase in Young's modulus in compression [5], observed also experimentally [6]. Thus, the term 'elastic constants' may be considered somewhat obsolete when regarding thermally sprayed coatings.

Another level of anisotropy stems from the crystalline structure within the splats. Directional heat removal during rapid solidification leads to formation of columnar grain structure [7].

This, together with the void system, causes anisotropic mechanical behavior beyond that caused by elastic anisotropy of the crystals [8].

Development of *residual stresses* in the deposits can be divided into two stages [9,10]. When the molten particles strike the substrate, they are rapidly quenched, while their contraction is restricted by adherence to the substrate. This leads to tensile stress in the deposit, commonly referred to as 'quenching stress'. During the deposition, the substrate is usually at some elevated temperature; during post-deposition cooling to room temperature, thermal mismatch stress develops due to difference in thermal expansion between the deposit and the substrate. Depending on the sign of this difference, the so-called 'thermal' stress can be tensile or compressive. Quenching and thermal stresses are two main contributions to the overall residual stress. There is an upper limit on stress imposed by the deposit cohesive and adhesive strength [11]. Their magnitude is generally dependent on the dimensions, thermal and mechanical properties of both the coating and the substrate and can be significantly influenced by the processing conditions (e.g., the deposition temperature [12]).

In the following sections, focused on each of the three features of thermally sprayed deposits, the application of neutron scattering/diffraction for their characterization will be discussed. The principle of each method will be outlined and its application on sprayed deposits will be described. Selected examples of recent experimental work will be provided, highlighting the advantages and capabilities of each method.

VOID STRUCTURE

Voids structure (Figure 2) of the thermally sprayed deposits is dominating factor influencing their mechanical, electrical and thermal properties. The three major components, described above have different influence on the properties of the deposits due to their different sizes, shapes and anisotropy. Therefore it is important to be able to quantify them and find relationships, which would allow designing the microstructures for particular applications.

Generally used techniques for description of the void system of these materials are volumetric intrusion measurements – mercury intrusion porosimetry or Archimedean water intrusion porosimetry – or image analysis using optical or scanning electron microscopy [13,14]. The former technique characterizes all voids in the sample by one number – porosity fraction, and cannot distinguish among different void systems. The later technique requires preparation of the cross sectional polished cut, which poses a challenge for many materials, especially for the thermally sprayed deposits, which usually exhibit high fragility. It is therefore clear, that while both of these techniques provide important insight into the materials structure, they need to be complemented by other techniques, providing more detailed description of the void system.

Small-angle scattering was selected as promising technique, since it provides information on the internal structure of the materials. And in case of small-angle scattering of neutrons, with high penetration capabilities of most materials, the sample sizes can be large and therefore the sample surface preparation becomes unimportant – in most cases the sample preparation is reduced to sectioning of the sample by diamond cutting wheel. Further advantage is, that the small-angle scattering resolution limit is in the order of few nanometers, which is significantly lower than for example image analysis technique.

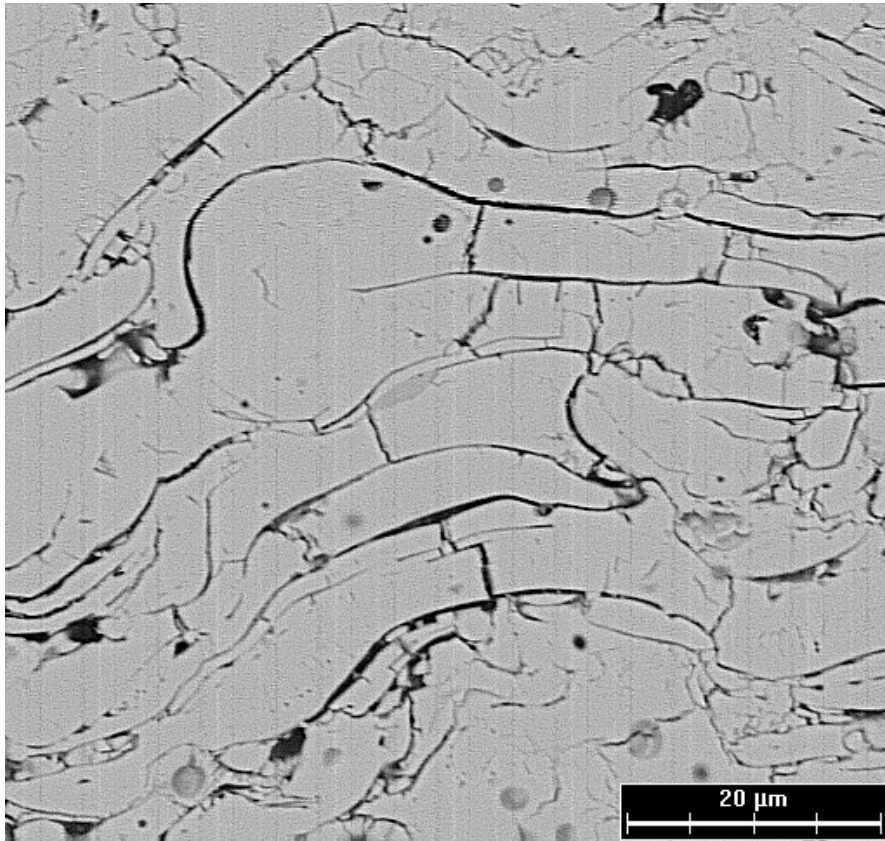


Figure 2: Microstructure of the Thermally Sprayed Yttria-Stabilized Zirconia. Note the three different void systems – clearly visible interlamellar pores, volumetric pores and, difficult to distinguish, intralamellar cracks.

Two basic small-angle neutron scattering techniques were developed for use on these materials up to date. Both are anisotropic variations of routinely used small-angle scattering techniques – so called Porod scattering [15] and multiple-small angle scattering [16]. Both take advantage of the special type of anisotropy in these materials – the samples look isotropic when viewed along the spray direction, while being highly anisotropic when viewed in the cross section.

Porod scattering is a standard small-angle scattering technique, which, for the isotropic materials, quantitatively characterizes the scatterers in the sample by their specific surface area. In the case of anisotropic materials the situation is more challenging. The usual relationship (through materials constants) between the specific surface area and measured Porod constant is valid only for 3-D average (i.e., over all 4π) of the Porod constant. Therefore to recover the calibrated specific surface areas one needs to know the average value of Porod constant, which effectively means knowing the scattering from the sample in all the directions. Taking advantage of the above-mentioned special type of sample anisotropy, the scattering in all directions from the sample can be reconstructed from just one measurement of the distribution of scattering in the cross section only (Figure 3).

It should be pointed out that the Porod scattering tends to significantly overestimate the anisotropy, so only mildly anisotropic scattering shapes exhibit strongly anisotropic distribution of Porod constants. Further it is important to note, that while it is possible to separate the scattering from the different void systems using the scattering anisotropy and average the data separately over all directions for each separate void systems, there is no

direct relationship between the scattering from the sample in any particular direction and the surface areas in that direction.

Anisotropic multiple small-angle scattering is significantly more challenging technique to describe and is beyond the scope of this paper. For details see [17].

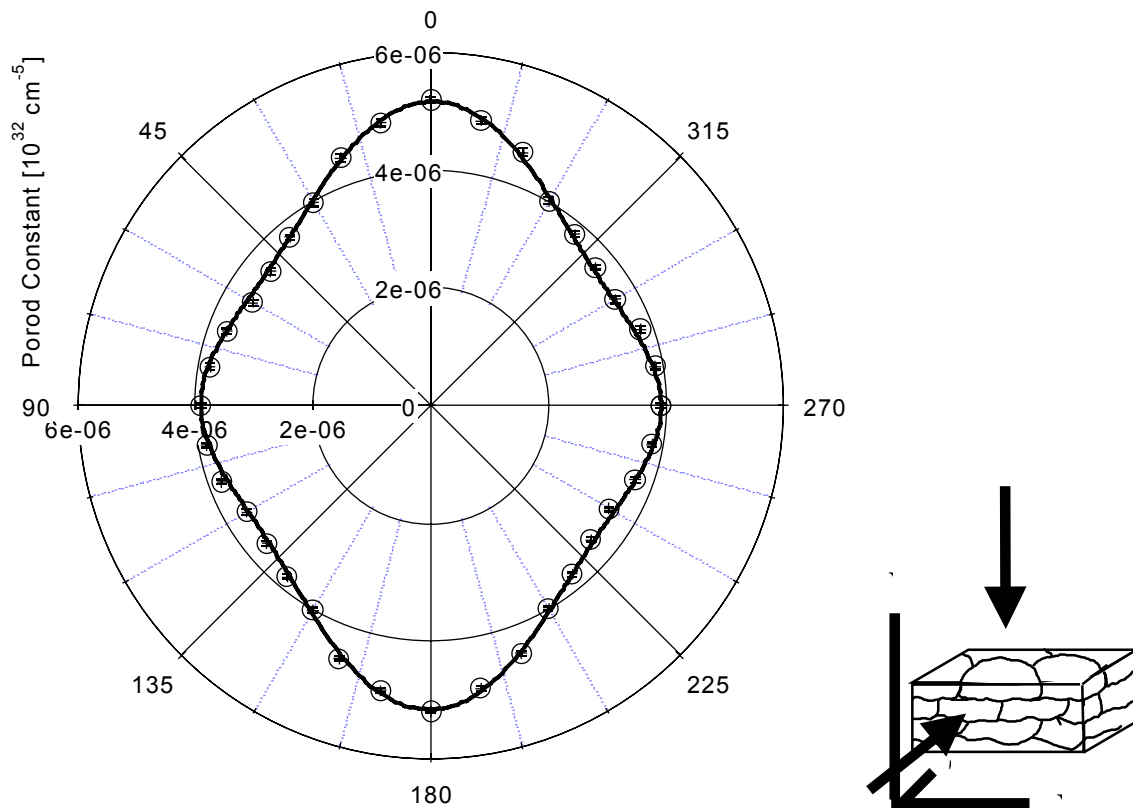


Figure 3: Distribution of Porod Constants measured in the cross section.

An example Porod scattering from the sample is in Figure 4. The three dimensional surface of the “ornament” in this figure represents the distribution of Porod constants or apparent Porod surfaces which could be obtained by measurement in any particular direction from the sample. This distribution is here called apparent Porod constant (or Porod surface) distribution, The Porod constant and Porod surface are proportional through scattering contrast of the scatterers.

The three dimensional structure in Figure 4a can be separated into two subsystems, Figure 4b and c, assuming that each system can be described as rotational ellipsoid. This is relatively simple assumption, but previous experiments suggest, that it can be reasonable. See Figure 5, which shows changes of the three dimensional apparent Porod constant distribution of the yttria-stabilized zirconia thermally sprayed deposits as sprayed and annealed. The measurements were done in situ. The changes show how the two-system distribution changes and the distribution becomes more and more resembling one ellipsoid. This was explained as preferential sintering of one of the systems (crack system) at lower temperatures.

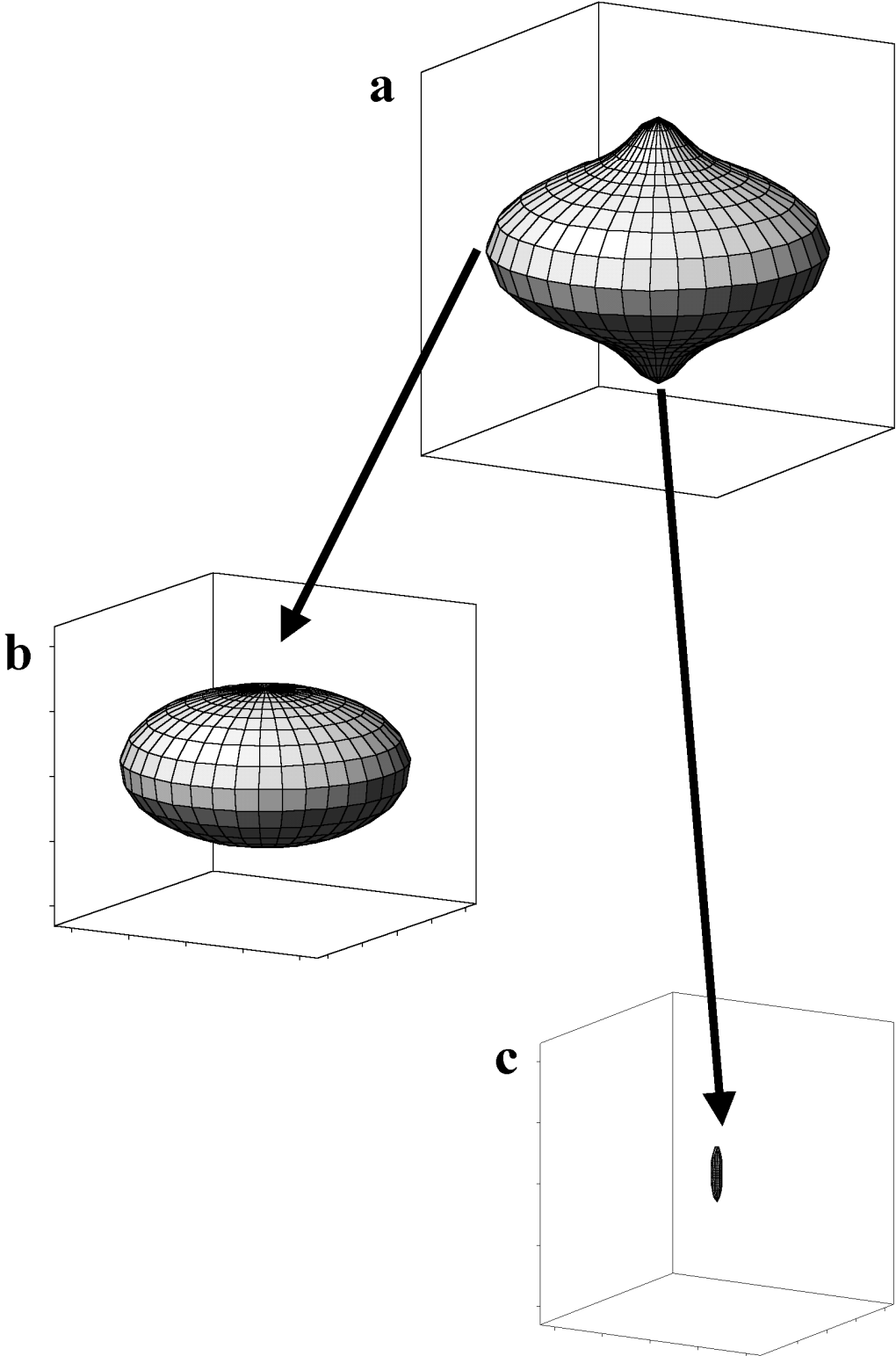


Figure 4. Three-dimensional reconstruction of Porod scattering from thermally sprayed sample.

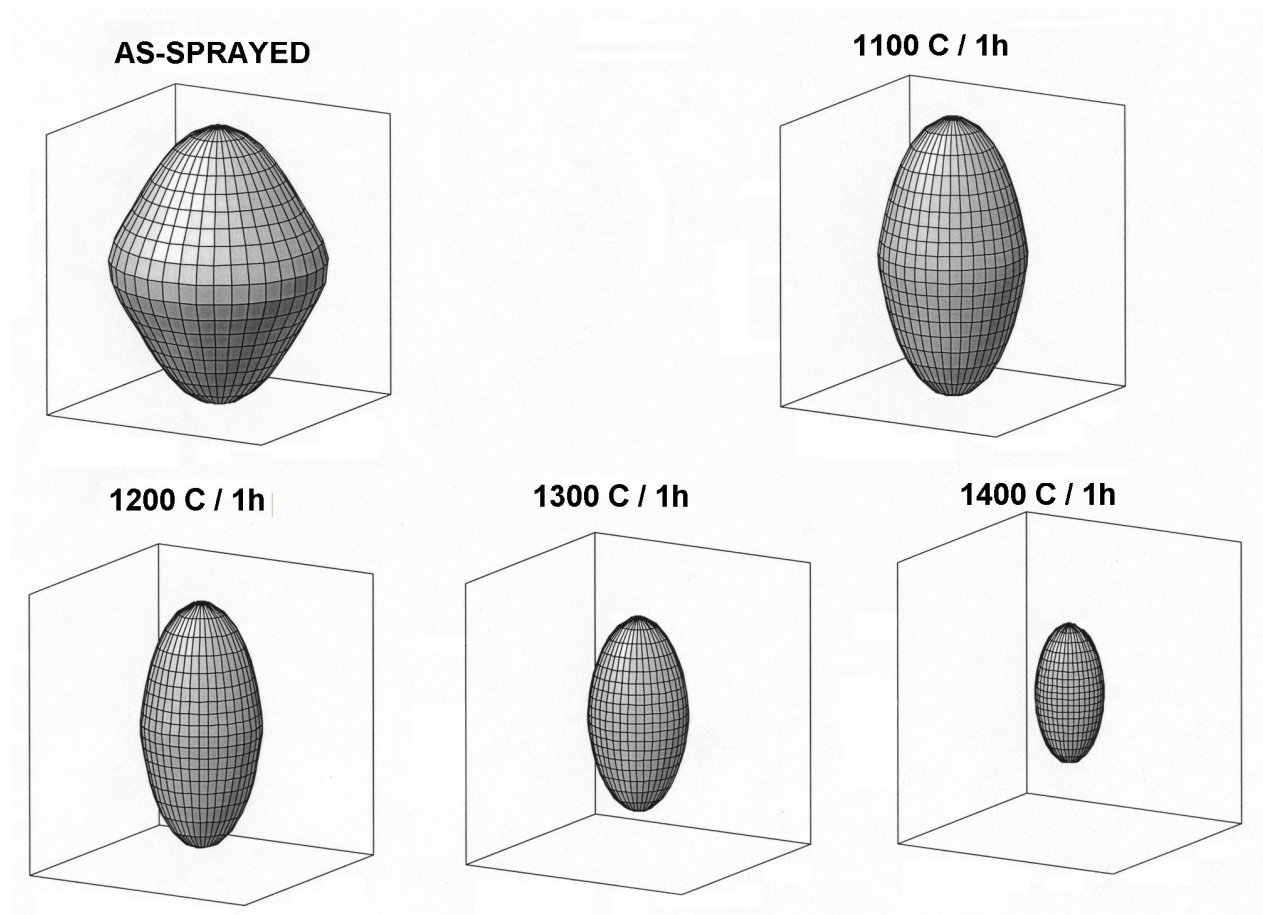


Figure 5. Development of the anisotropic scattering from the sample annealed at increasing temperatures. The change is related to preferential sintering of one of the void systems (intralamellar cracks). From [18].

The description of the void system by the distribution of the apparent Porod constants and by values of the specific surface areas for separate void subsystems is significant improvement of the “porosity” value measured by intrusion techniques and by image analysis. However, there are limitations, which are inherent to this method. Mainly, one of the major void systems is not distinguished – the large mostly globular voids, which may have significant volume but due to their large size they have relatively small surface area. And of course, since this void system is roughly isotropic, these small surfaces cannot be identified in the distribution of apparent Porod constants or surfaces. Further more, if the other two major void systems do not exhibit enough anisotropy, it is impossible to reliably separate them and only one specific surface area for the sample can be obtained.

More detailed description of the void system is possible by combining of the anisotropic Porod surfaces and anisotropic multiple small-angle scattering technique (and standard techniques). These techniques were successfully applied for studies of ceramic (YSZ) deposits [17] and the void systems were separated – and each characterized by average opening, overall volume and specific surface area. Such description, even though based on void system model, is unique and shows how the small-angle scattering technique can be used for microstructure characterization of the anisotropic void system.

Elastic properties

As mentioned before, the presence of pores with a concentration of up to 10% significantly alters the mechanical properties of the coating with respect to those of the bulk material. The measurement of the elastic moduli is usually done by four-point bending, indentation or sometimes by ultrasonic resonance. Each of these methods comes with its own restrictions but all of them have in common that they provide only results for Young's modulus parallel and perpendicular to the coating plane. So far, there are no data available about Poisson's ratios and the shear modulus.

In this context, neutron diffraction offers an interesting alternative to the measurement methods mentioned above because it is a strain measurement which means that by recording the strain in dependence on the applied load Poisson's ratios and the two Young's moduli can be obtained directly. This is done by measuring the expansion or contraction of the coating material with applied stress and for different coating orientations. For example, Young's modulus perpendicular to the coating plane is obtained by applying a stress perpendicular to the coating plane and by measuring the lattice strain in the same direction. Fig. 6 shows a schematic of the device used in such an experiment.

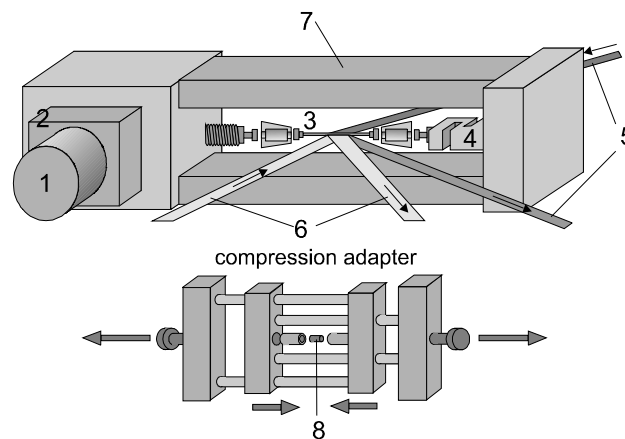


Figure 6: Stress rig used for measuring elastic constants by neutron diffraction. The components are: 1) stepper motor; 2) reduction gear; 3) tensile sample; 4) load cell; 5) in and outgoing neutron beam for measuring Young's modulus; 6) neutron beams for measuring Poisson's ratio; 7) frame; 8) compression sample.

However, the values obtained that way depend to a certain extent on the elastic anisotropy of the crystallites which constitute the coating; in other words, the results depend on the Miller indices of the reflection that was used in the diffraction measurement. Another important aspect of this kind of measurement is that only the *elastic* strain of the coating material is measured. As a consequence, any part of the strain

is omitted that goes into the deformation of cracks and voids or as plastic strain in the case of metallic coatings. Generally, the elastic constants measured by diffraction on the actual coating material will be lower than those of the bulk material (without porosity) and higher than the elastic constants of the coating as a whole (which includes the pores).

The diffraction moduli and the overall coating moduli are correlated by the elastic interaction of pores and coating material. The relationship between both – if known – can then be used to calculate the overall coating moduli from the diffraction moduli [8]. Examples for that are shown in Table. 1 [8].

Table 1. Young's modulus and Poisson's ratio in specimen directions normal (\perp) and parallel (\parallel) to the coating surface for a nickel coating and a yttria stabilized zirconia (YSZ) coating. The values were calculated from the hkl -dependent moduli obtained from diffraction in a compression experiment. Values are given in units of GPa. ν^\perp indicates Poisson's ratio for a stress applied perpendicular to the coating plane; there are two Poisson's ratios if the stress is applied parallel to the coating plane: ν^\parallel parallel to the coating plane (normal to the stress) and $\nu^{\parallel\perp}$ perpendicular to the coating plane. The total porosity of the nickel coating is 10%; the porosity of YSZ is 11%.

coating	E^\perp	E^\parallel	ν^\perp	ν^\parallel	$\nu^{\parallel\perp}$	μ
Ni	149 (15)	118 (14)	0.35 (0.1)	0.28 (0.1)	0.47 (0.1)	97 (10)
YSZ	83 (20)	185 (20)	0.25 (0.12)	0.49 (0.2)	0.1 (0.1)	59 (10)

The model that was used in these calculations [8] is strictly linear and it does not allow for internal friction and closing of pores with increasing stress. Thus, the model tends to overestimate the coating elastic constants as compared to results obtained from bending and indentation as shown in Table 2.

Table 2. Values for Young's modulus as obtained by other methods. Values are given in units of GPa. Those marked with an asterisk were taken from ref. [19], the value marked with a '+' was obtained by bending. E_{bulk} was calculated for isotropic polycrystals.

specimen	E_{meas}^\perp	$E_{\text{meas}}^\parallel$	E_{bulk} (no pores)
Ni	-	78 (6) ⁺	232
YSZ	21.9 (1.9)*	37.0 (4.5)*	219

While it is clear that the porosity, the shape and the distribution of pores/cracks are the most important factors that determine the coating elastic constants, it is difficult to assess this correlation quantitatively. Real distributions of orientations and aspect ratios of pores/cracks are difficult to obtain, and it is also not clear to what extent the microstructure can be idealized with pores of a certain shape and orientation. However, some of these problems can be approached experimentally. As an example, we consider two coatings air plasma sprayed under the same conditions with the same material (Inconel 737, expected to be similar to NiCrAlY) but with different particle sizes. Both samples were subjected to in-situ four point bending tests in which the lattice strain was measured by means of neutron diffraction. The feedstock powders were obtained by sieving which sets a rather narrow range for the particle size. The particle size of the "coarse" powder was $116 \pm 9 \mu\text{m}$; the particle size of the "medium" powder was $68 \pm 5 \mu\text{m}$.

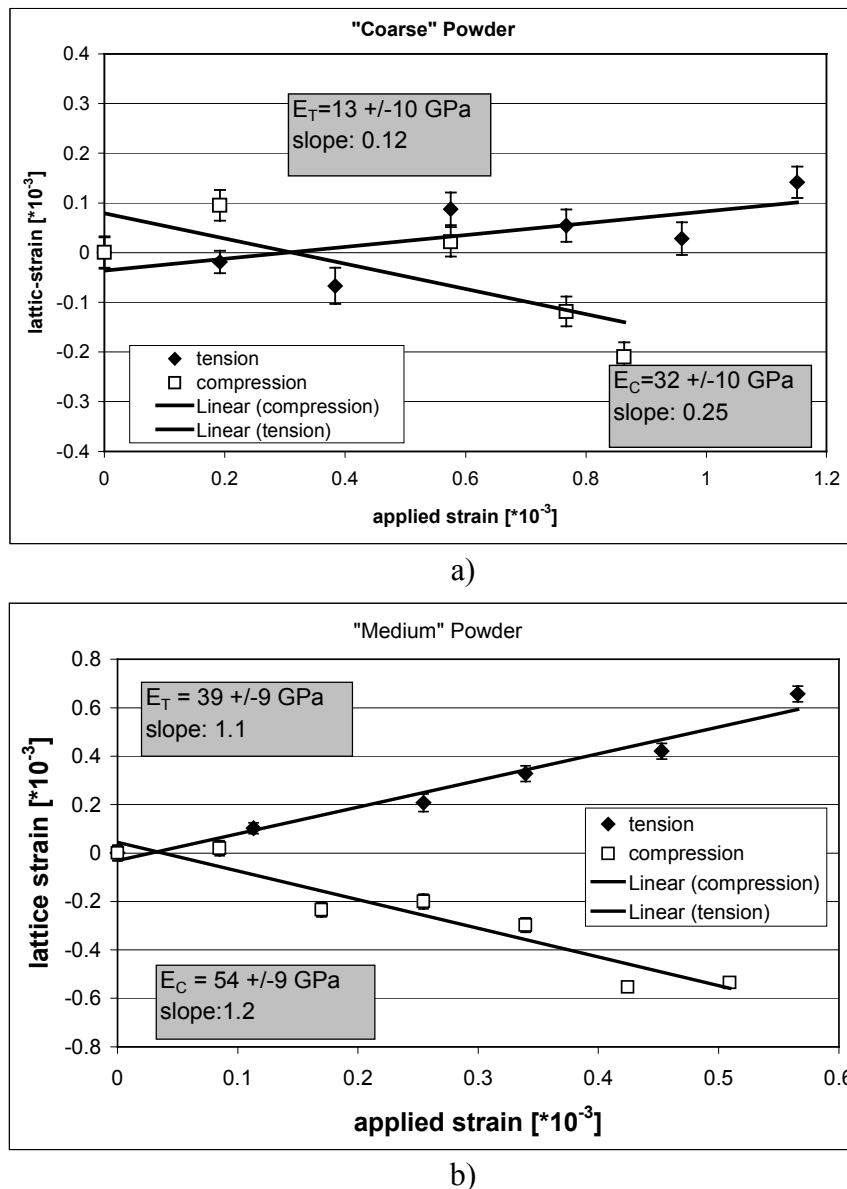


Fig. 7. Lattice strain (from diffraction) over applied strain (from bending curvature) for a) the coarse powder and b) the medium powder. The values for Young's modulus in tension (E_T) and in compression (E_C) were obtained from the measured bending force and the bending strain. Both the applied strain and the lattice strain are average strains, i.e. the applied strain was calculated for the middle of the coating thickness and the lattice strain is the through-thickness average as measured by neutron diffraction on the (311) reflection.

Figure 7 indicates that essentially a 50% drop in particle size effectively doubles the in-plane modulus of the coating. Also, the fraction of the applied strain that goes into the lattice strain (slopes) increases by a factor of five (compression) to ten (tension) for the smaller particles. The relative difference between the moduli in compression and in tension also decreases with decreasing particle size. As indicated by the slopes (approximately equal to 1) of the linear regression curves for the medium coating, the lattice strain follows the applied strain ideally. The slopes having values >1 are a consequence of the (311) diffraction modulus being elastically softer than the average modulus for Inconel 737. This finding gives evidence that the total porosity of the medium coating is significantly less than that of the coarse coating.

Preliminary results from small angle neutron scattering experiments show that the surface area of the medium coating is slightly higher than that of the coarse coating. The connected porosity, on the other hand, is approximately five times higher for the coarse coating. A connection between elongated voids of the same orientation effectively increases the aspect ratios of the average void which has a significant impact on the elastic constants as shown in Figure 8.

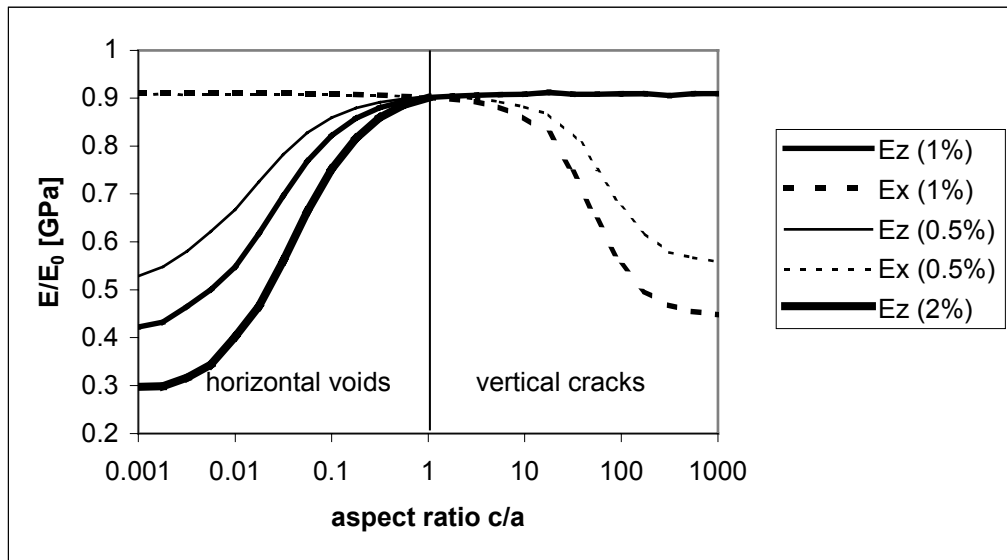


Fig. 8. Calculated effect of ellipsoid aspect ratio and concentration of elongated voids on Young's modulus perpendicular (E_z) and parallel (E_x) to the coating plane. The modulus E_x does not depend on direction within the coating plane. Each curve represents Young's modulus for a material with two void populations – spherical voids with concentrations of 8%, 9% and 9.5%, and elongated, “penny shaped” voids with concentrations of 2%, 1% and 0.5%, respectively. The total porosity is assumed to be 10%.

The most significant impact of the pore aspect ratio on the elastic moduli is caused by values between 0.1...0.01 and 10...100, respectively. The 50% drop in elastic constants can be well explained by assuming that the average pore aspect ratio for the coarse coating is five times larger than that of the medium coating due to increased connection between pores.

These results demonstrate that neutron diffraction can give a more detailed insight into the elastic behavior of coatings not only in terms of measuring elastic constants but also by providing information about the microstructural properties of the coatings that are responsible for the decrease and the anisotropy of the coating elastic constants.

RESIDUAL STRESS

Overview. The most popular methods of residual stress determination in coatings can be roughly divided into three groups: material removal methods, substrate curvature measurement and diffraction methods. A detailed overview was given in [20]. Neutron diffraction holds a specific position among the stress determination methods, thanks to a number of advantages:

- it is nondestructive;
- it can determine stresses in individual phases of a multi-phase system;
- it has very relaxed requirements on specimen size and shape;

- due to high penetration of neutrons (compared to x-rays), stresses can be determined inside thick deposits as well as substrates without any material removal; this includes triaxial stress states;
- the specimens could have undergone inelastic deformation.

Among the disadvantages are lower spatial resolution (compared to other methods) and limited availability of experimental facilities.

Diffraction methods of stress determination are based on measurement of changes in crystal plane spacing in different directions with respect to the specimen surface, which exhibit themselves as shifts in angular positions of respective diffraction peaks. From thus obtained strain, stress can be calculated with the use of appropriate elastic constants. An overview with the necessary formulae can be found elsewhere [21]. Specifics of application of neutron diffraction on coatings will be described here, based on an actual instrument used in our experiments, i.e., the DARTS diffractometer at NIST [22] – see schematic on Figure 9a.

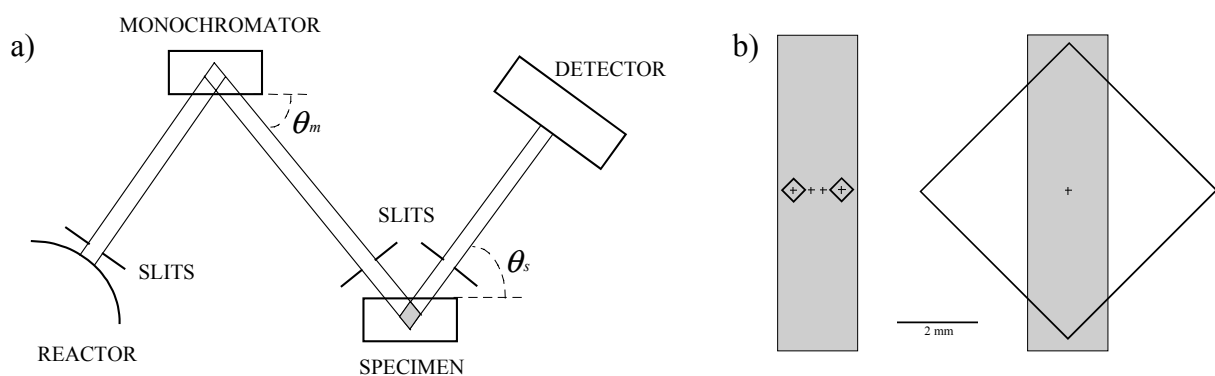


Fig. 9. Schematic of the neutron diffraction measurement. a) experimental setup; θ_m - diffraction angle at the monochromator, θ_s - diffraction angle at the specimen; grey-shaded diamond indicates the gauge volume; b) two different cases of gauge volume size with respect to specimen thickness - small gauge volume for through-thickness profiling, larger gauge volume for average values from the entire thickness [23].

From a polychromatic beam of neutrons, a desired wavelength was selected by diffraction on a monochromator crystal (the wavelength being defined by the crystal's lattice spacing and diffraction angle). The monochromatic beam illuminating the specimen was diffracted and detected by a position sensitive detector. Two apertures, one before and one after the specimen defined the size of incident and diffracted beams. Their intersection defines the "gauge volume" - the volume being probed by the neutrons (see Fig. 9b). For thick deposits, the gauge volume in our experiments was $1 \times 1 \times 7 \text{ mm}^3$, which permitted the determination of through-thickness stress gradients. In cases when the gauge volume was only partially filled with the diffracting material (near-surface measurement), the artificial peak shifts thus generated were quantified on annealed (stress-free) specimens and subtracted from other experimental data [23]. For thinner coatings, where small gauge volume inside the material would not give a practical flux of diffracted neutrons, a gauge volume larger than the specimen thickness was chosen and the diffracting material was centered in this volume so that the surface effects would cancel each other. This way, only an average value from the entire coating thickness could be obtained. Due to specimen geometry (planar coatings), the assumption of zero stress perpendicular to the coating plane could be used, thus reducing the number of necessary measurements in different orientations.

Example – comparison with other methods. In this example, residual stresses in nickel coatings sprayed by atmospheric (APS) and vacuum plasma spraying (VPS) on steel

substrates were determined by x-ray diffraction, neutron diffraction and hole-drilling. Details of the specimen preparation and measurements were given in [24]. The coating thicknesses were 0.1 and 0.6 mm, respectively. The results are presented in Table 3.

Table 3. Residual stresses in APS and VPS nickel coatings, determined by various methods. XRD = x-ray diffraction, HD = hole-drilling, ND = neutron diffraction, σ = in-plane stress. Standard deviations were in the 10 – 20 MPa range.

Specimen	Ni-APS	Ni-VPS
Method	σ (MPa)	σ (MPa)
XRD	62	-116
HD	241	-55
ND	186	-37

As can be seen, all three methods yielded qualitatively comparable results, although the magnitudes were different. The origin of these differences lies in a) the nature of primarily measured quantity and b) the probed volume. While the diffraction methods measure strain in coherently diffracting crystalline domains, the “macroscopic” strain measured by hole drilling may encompass crack opening and intersplat sliding. This can explain the higher magnitude of the HD data compared to those from neutrons and from x-rays on the APS sample. Neutron diffraction measures the same quantity as x-ray diffraction, but over a different volume - the ND values reported in Table 3 are averages over the entire coating thickness, while the XRD values come from a thin surface layer. Thus, the lower stress value observed in APS using XRD could be explained by surface roughness relaxation. On the other hand, higher XRD stress value in the VPS coating (whose surface was polished) could be a result of a through-thickness stress gradient. Such stress gradients over the coating thickness are typical of thermally sprayed coatings (see next paragraph).

The opposite stress sign in the APS and VPS coatings is caused by a difference in deposition temperature. In APS, the deposition temperature is lower and the tensile quenching stress is retained in the coating. In VPS, higher deposition temperatures are reached, which lead to self-annealing of the coating during deposition. Thus, the residual stress is dominated by the (compressive) thermal stress component.

Example – through-thickness stress profiles. This example demonstrates the capability of this method to determine stress gradients throughout the entire coating and substrate, without any material removal. The specimen was a 2 mm thick plasma sprayed Ni+5%Al alloy on a 2.5 mm steel substrate. Details of the specimen preparation and measurements were given in [25]. The results are shown in Fig. 10. The overall stress in the coating is slightly tensile, with a gradient towards tension near the deposit surface, as a result of successive buildup of deposit layers with tensile quenching stress. The stress in the deposit is accommodated by bending of the substrate, as indicated by the gradient from tension on the back surface to compression at the substrate/deposit interface. For this deposit/substrate material combination, the thermal mismatch is very small, therefore the residual stress profile results mainly from the quenching stress. In a material combination with higher thermal mismatch (e.g., molybdenum/steel), the thermal stress component would be dominating [12].

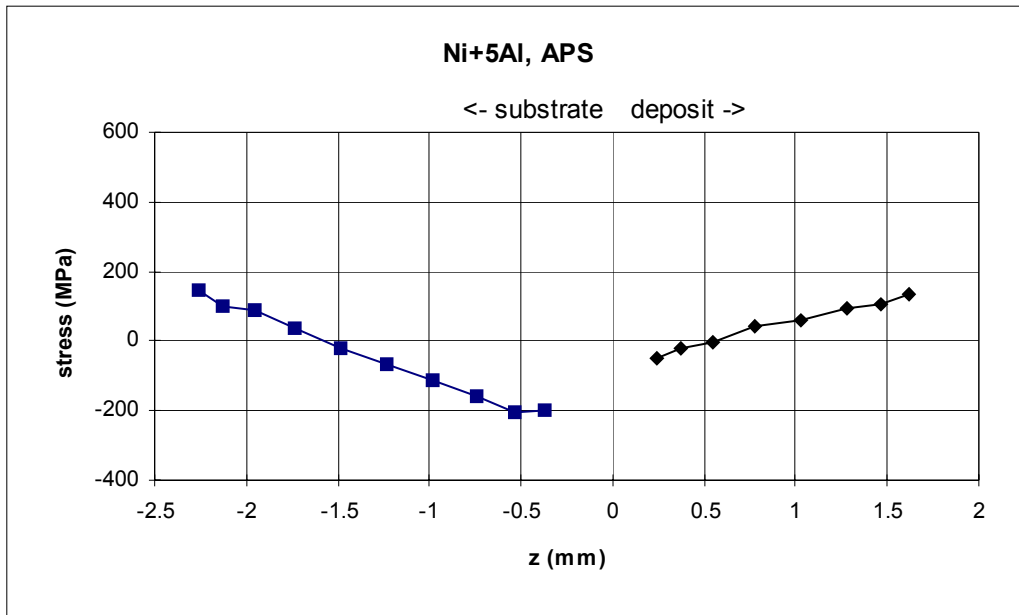


Fig. 10. Through-thickness profile of the residual stress in plasma sprayed Ni+5Al deposit and steel substrate. Standard deviations for the stress in the deposit ranged from 8 MPa in the middle to 16 MPa near the surfaces, for the substrate from 5 MPa in the middle to 10 MPa near the surfaces [25].

Example – phase stresses. Figure 11 illustrates the unique capability of neutron diffraction to determine stresses in individual phases of a multi-phase material. Residual stresses in the YSZ and NiCrAlY phase of plasma sprayed YSZ+NiCrAlY composites with varying composition [26] are shown. One can see that the stress in the metallic phase is tensile and in the ceramic phase it is compressive; this comes from lower thermal expansion of zirconia than those of NiCrAlY and steel. The respective magnitudes increase with decreasing content of the phase. Coating stress is balanced by that in the substrate.

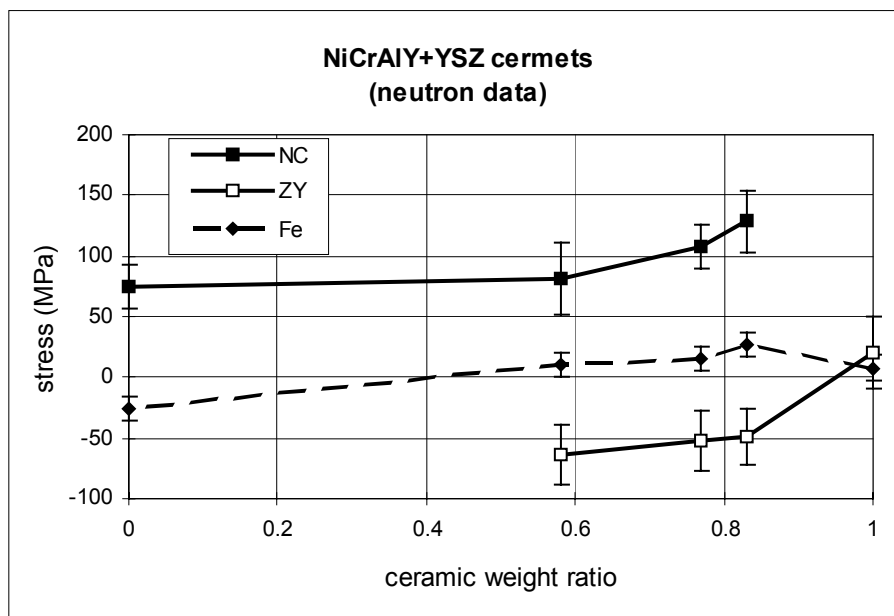


Fig. 11. Residual stresses in YSZ+NiCrAlY cermets - data from individual specimens of given composition [26]. Average stresses in each phase of the coating, as well as the substrate, are shown.

CONCLUSIONS

Neutron scattering and diffraction are powerful techniques for characterization of materials structure and properties. They have certain unique capabilities that cannot be achieved by other methods. These capabilities were demonstrated through case studies of highly complex anisotropic materials – thermally sprayed coatings. Their void structure, elastic properties and residual stresses were characterized by neutron scattering and diffraction, respectively. All these properties are important factors in possible failure processes in these coatings, their performance and lifetime.

REFERENCES

- [1] Pawlowski, L.: *The Science and Engineering of Thermal Spray Coatings*; Wiley & Sons, Chichester, 1995.
- [2] McPherson R.: *Surf. Coat. Tech.*, 39-40, 1-3 (1989) 173.
- [3] McPherson R.: *Ceramics-Silikáty*, 35 (1991) 273.
- [4] Li C. J., Ohmori A. and McPherson R.: *J. Mater. Sci.* 32, 4 (1997) 997.
- [5] Kroupa F. and Dubský J.: *Scripta materialia* 40, 11 (1999) 1249.
- [6] Harok V. and Neufuss K.: *J. Thermal Spray Tech.* (2001) in press.
- [7] McPherson R. and Shafer B. V.: *Thin Solid Films*, 97, 3 (1982) 201.
- [8] Gnäupel-Herold T., Matějček J. and Prask H. J.: In: *Proc. 9th Intl. Metallurgical Conf. Metal2000*, T. Prnka (Ed.). Tanger, Ostrava, 2000, paper no. 508.
- [9] Clyne T. W., Gill S. C.: *J. Thermal Spray Tech.* 5, 4 (1996) 401.
- [10] Kroupa F.: *Acta Technica ČSAV* 42, 5 (1997) 591.
- [11] Kuroda S., Fukushima T. and Kitahara S.: In: *Proc. Int. Thermal Spray Conf.*, C. C. Berndt (Ed.). ASM, Materials Park, 1992, pp. 903-909.
- [12] Matějček J., Sampath S. and Herman H.: In: *Proc. 15th Intl. Thermal Spray Conf.*, C. Coddet (Ed.). ASM, Materials Park, 1998, pp. 419-424.
- [13] Ilavský J., Berndt C. C. and Karthikeyan, J.: *J. Mater. Sci.* 32, 15 (1997) 3925.
- [14] Ilavský J., Long G. G., Allen A.J., Leblanc L., Prystay M. and Moreau C.: *J. Thermal Spray Tech.* 8, 3 (1999) 414.
- [15] Kostorz G.: In: *Treatise on Materials Science and Technology*, 15 (1979) pp. 1-289.
- [16] Berk N. F. and Hardman-Rhyne K. A.: *J. Appl. Cryst.* 21 (1988) 645.
- [17] Allen A. J., Ilavský J., Long G. G., Wallace J., Berndt C. C. and Herman H.: *Acta Materialia* 49, 9 (2001) 1661.
- [18] Ilavský J., Long G. G., Allen A.J., Berndt C. C. and Herman H.: In: *Proc. 1st United Thermal Spray Conference*, C. C. Berndt (Ed.). ASM, Materials Park, 1997, 697.
- [19] Wallace J. S. and Ilavský J.: *J. Thermal Spray Tech.* 7, 4 (1998) 521.
- [20] Matějček J.: In: *Proc. 9th Intl. Metallurgical Conf. Metal2000*, T. Prnka (Ed.). Tanger, Ostrava, 2000, paper no. 510
- [21] Allen A. J., Hutchings M. T., Windsor C. G. and Andreani C.: *Adv. Phys.* 34, 4 (1985) 445.
- [22] Prask H. J. and Brand P. C.: *Mater. Sci. Forum* 210-213 (1996) 155.
- [23] Matějček J., Sampath S., Brand P. C. and Prask H. J.: *Acta Materialia*, 42, 7 (1999) 607.
- [24] Matějček J., Sampath S. and Dubský J.: *J. Thermal Spray Tech.*, 7, 4 (1998) 489.
- [25] Matějček J., Sampath S., Gnäupel-Herold T. and Prask H. J.: In: *Proc. 1st Intl. Thermal Spray Conf.*, C. C. Berndt (Ed.). ASM, Materials Park, 2000, pp. 351-354.
- [26] Kesler O., Matějček J., Sampath S., Suresh S., Gnäupel-Herold T., Brand P. C. and Prask H. J.: *Mater. Sci. Eng. A* 257, 2 (1998) 215.